Chapter 1

Nucleosynthesis of Elements in Stars

"The elements from carbon to nickel have been synthesized in stars."

F. Hoyle (1954)

Lecture 27 closed with hydrogen burning in the Sun and with solar neutrinos as core diagnostics. That process explains only the first step of elemental history: $4p \to {}^4\text{He}$. The Periodic Table contains roughly ninety stable elements and about three hundred stable nuclides. Their origins define **nucleosynthesis**: Big Bang production of the lightest species, followed by stellar fusion building nuclei up to the iron group, and neutron capture beyond the iron peak [6, 1, 14, 37, 32].

The logic of the chapter is causal rather than encyclopaedic. First one must understand why the early Universe stops at lithium; then why cosmic abundances show a gap at Li–Be–B and a peak at iron; then how helium burning bridges that gap via the Hoyle resonance; and finally how massive stars climb the binding-energy curve until fusion ceases and neutrons take over.

1.1 Two stages of nucleosynthesis

Hydrogen and helium still dominate the baryonic mass of the Universe, approximately 75% and 25% by mass, almost unchanged from the values set a few minutes after the Big Bang. Heavier species make up only about 1% of that budget, yet they include the carbon, oxygen, silicon and iron needed for planets and chemistry [14, 6]. Two physically distinct epochs produce them.

Big Bang nucleosynthesis (BBN) operates in an expanding, cooling radiation-dominated plasma. Temperatures fall from MeV to $\sim 0.1\,\text{MeV}$ in minutes. Reactions that require three-body collisions, long confinement, or slow penetration of a high Coulomb barrier simply do not have time. The stable products are almost only ${}^1\text{H}$ and ${}^4\text{He}$, with traces of d, ${}^3\text{He}$ and ${}^7\text{Li}$ ($A \le 7$). Nothing beyond lithium is made in significant quantity [14, 6].

Stellar nucleosynthesis begins once gravity confines primordial gas in galaxies and stars. Hydrostatic and explosive burning then manufacture carbon through the iron group; neutron captures later reach the heavier species [37, 6]. Solar spectroscopy of dozens of photospheric elements samples galactic material already enriched by earlier stellar generations [14]. The Sun itself is a late generation star: its metals (everything heavier than helium, in astronomical usage) were forged elsewhere.

1.2 Cosmic abundances as a nuclear map

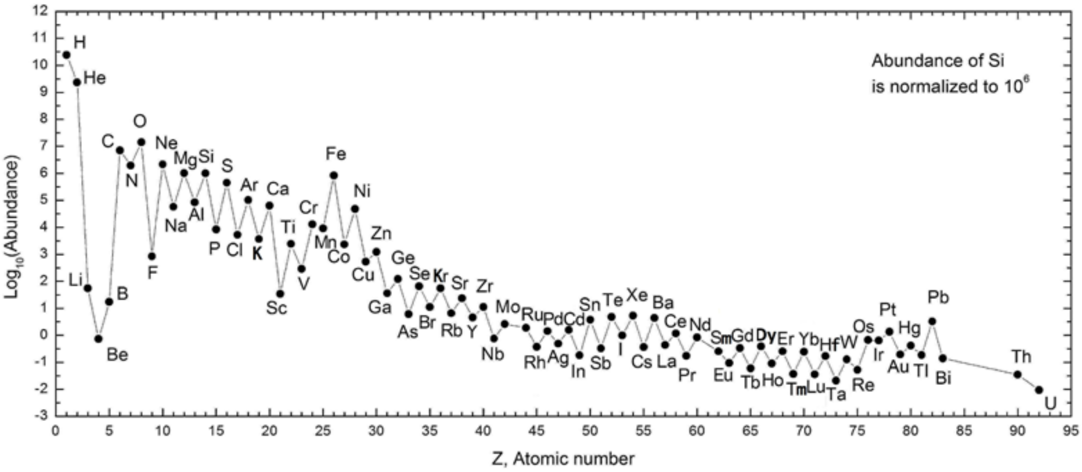

Figure 1.1: Solar-system elemental abundances (logarithmic scale). Hydrogen and helium dominate; Li–Be–B are strongly suppressed; even-Z peaks and an iron-group hump structure the rest of the chart. Image: Wikimedia Commons ("SolarSystemAbundances.png"), CC BY-SA 3.0 [14, 6].

Figure 1.1 is not merely a table of abundances; it is a nuclear fingerprint of the channels that operate in Nature [14, 6, 37].

Hydrogen and helium dominate. Even after $\sim 10^{10}$ years of stellar processing, baryonic matter remains mostly primordial. Stars convert H to He and He to heavier nuclei, but most of the cosmic baryon inventory never passes through a stellar core. That is why the BBN prediction $Y_{\mathrm{He}} \approx 0.25$ still matches the observed helium mass fraction to high accuracy.

Lithium, beryllium and boron are rare. Between helium ($A = 4$) and carbon ($A = 12$) there is no stable $A = 5$ or $A = 8$ nucleus that can serve as a steady stepping stone for charged-particle fusion. Cosmic LiBeB therefore cannot be primary ashes of hydrostatic helium burning; they arise mainly from cosmic-ray spallation of CNO nuclei and from limited Big Bang ^{7}Li. The deep trough at $Z = 3$–5 on Fig. 1.1 is the abundance signature of that mass gap.

Even–odd staggering. Even-Z and even-N nuclei are systematically more abundant than their odd neighbours. Pairing in the SEMF and the tendency of nucleons to cluster into α-like subunits favour even–even species; reaction networks that proceed by α capture inherit that preference.

Iron-group peak. The binding energy per nucleon B/A is maximal near $A \sim 56$–62. Charged-particle fusion therefore releases energy while climbing toward that peak and ceases to power a star beyond it (Sec. 1.7). The abundance hump at iron is the endpoint of exothermic fusion, visible already in the empirical B/A curve of Lecture 25.

Secondary abundance peaks near $A \sim 80$, 130 and 195 are not explained by charged-particle fusion; they are the fingerprints of neutron capture at closed neutron shells (previewed in Sec. 1.9).

1.3 Big Bang nucleosynthesis

1.3.1 Weak freeze-out and the n/p ratio

At temperatures $k_BT \gg 1\,\text{MeV}$, neutrons and protons remain in weak equilibrium through

$$n + \nu_e \leftrightarrow p + e^-, \qquad n + e^+ \leftrightarrow p + \bar{\nu}_e. \tag{1.1}$$

Detailed balance then fixes

$$\frac{n_n}{n_p} = \exp\Big(-\frac{\Delta m\, c^2}{k_BT}\Big), \qquad \Delta m\, c^2 \approx 1.293\,\text{MeV}. \tag{1.2}$$

As the Universe expands, the weak rates eventually fall below the Hubble rate (weak freeze-out, $k_BT \sim 0.8\,\text{MeV}$). The ratio freezes near $n_n/n_p \sim 1/6$. Free-neutron β decay continues until nucleosynthesis begins, leaving a neutron mass fraction $X_n \equiv n_n/(n_n + n_p)$ of order 0.12–0.13.

1.3.2 Helium mass fraction

Almost every surviving neutron ends in ^{4}He. If two neutrons (with two protons) form one α particle, the helium mass is $2n_n$ while the total baryon number density is $n_n + n_p$, so

$$Y_{\text{He}} \approx \frac{2X_n}{1 + X_n} \approx 0.25 \tag{1.3}$$

for $X_n \approx 1/7$–$1/8$ after the network is integrated [14, 6]. The complementary hydrogen fraction is $X_{\text{H}} \approx 1 - Y_{\text{He}} \approx 0.75$. Equation (1.3) is the cleanest example in the course of an observationally tested nuclear cosmology formula: the number of free neutrons at freeze-out sets the cosmic helium abundance.

1.3.3 Deuterium bottleneck and the $A \leq 7$ freeze

The deuteron binding is only $B_d = 2.224\,\text{MeV}$. While the radiation bath still contains a high-energy Maxwellian tail, photodisintegration $d + \gamma \to p + n$ destroys deuterium as fast as it forms (the **deuterium bottleneck**). Only when k_BT falls to $\sim 0.1\,\text{MeV}$ can deuterium survive long enough for the strong network

$$d(p,\gamma)^3\text{He}, \quad {}^3\text{He}(d,p)^4\text{He}, \quad {}^3\text{He}(^3\text{He}, 2p)^4\text{He}, \ldots \tag{1.4}$$

to lock remaining neutrons into ^{4}He, with tiny leftovers of d, ^{3}He and ^{7}Li [14, 6]. Expansion then freezes the network. Because no stable $A = 5, 8$ nucleus exists, BBN cannot climb to carbon: that step requires the sustained density of a stellar helium core.

1.4 From hydrogen burning to a helium core

Main-sequence stars convert hydrogen to helium by the *pp* chains and/or the CNO cycles of Lecture 27. In the Sun the *pp* path carries most of the luminosity; CNO contributes only a few percent at $T_c \sim 1.5 \times 10^7$ K. More massive (hotter) stars burn predominantly by CNO because the larger Coulomb barriers are offset by a higher Gamow peak [1, 36, 6].

As central hydrogen is exhausted, a helium ash core grows. Without nuclear energy generation that core contracts and heats under gravity (virial theorem), while the envelope may expand into a red-giant configuration [14]. Helium ignition occurs only if the core temperature and density reach the triple-α regime ($\sim 10^8$ K, $\rho \sim 10^5\,\mathrm{g\,cm^{-3}}$). A solar-mass star never proceeds through the full carbon–silicon sequence discussed below; those stages require more massive cores capable of successive gravitational heating after each fuel is exhausted [14, 6].

1.5 The triple-α process and helium burning

Figure 1.2 summarises the nuclear logic of helium burning: an equilibrium of unbound ^{8}Be, resonant capture into the Hoyle state of ^{12}C, and a rare radiative branch that locks carbon.

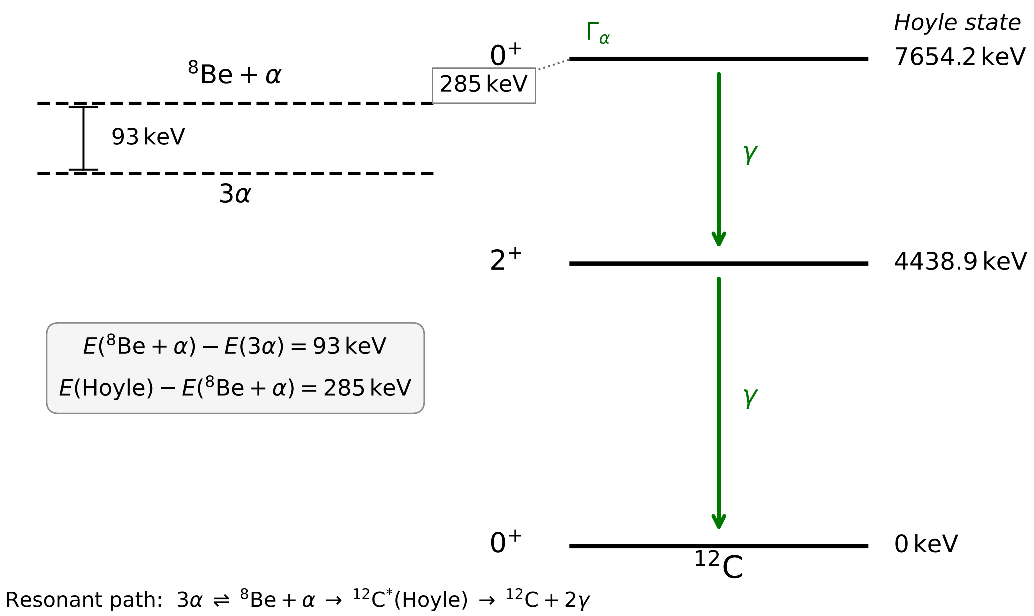

Figure 1.2: Level scheme for the triple-α process (redrawn; energies as in Wikimedia *Hoyle state and possible decay way*, CC BY-SA 4.0). Unbound ^{8}Be sits ≈ 92 keV above 2α; the Hoyle 0^+ of ^{12}C (7.654 MeV) lies ≈ 285 keV above the $^8\mathrm{Be}+\alpha$ threshold and radiates via 2^+ (4.439 MeV) to the ground state [38].

1.5.1 Why two-body α fusion fails

There is no exothermic two-body reaction among α particles alone. The mass of ^{8}Be exceeds twice the α mass by

$$|Q| = \left[m(^8\mathrm{Be}) - 2m(^4\mathrm{He})\right]c^2 \approx 92\,\mathrm{keV}, \tag{1.5}$$

so ^{8}Be decays back to 2α with $\tau \sim 10^{-16}$ s [14, 1]. Production is therefore reversible,

$$^4\mathrm{He} + {}^4\mathrm{He} \rightleftharpoons {}^8\mathrm{Be}. \tag{1.6}$$

Unlike the irreversible conversion of hydrogen to helium, helium burning must work with a tiny equilibrium population of an unbound intermediate.

1.5.2 Thermal equilibrium abundance of ^{8}Be

Applying chemical equilibrium (detailed balance) to (1.6) with reduced mass m of the α–α system yields the Saha-like ratio

$$\frac{n(^8\mathrm{Be})}{n(^4\mathrm{He})} = n(^4\mathrm{He}) \left(\frac{2\pi\hbar^2}{m\, k_B T} \right)^{3/2} \mathrm{e}^{-92\,\mathrm{keV}/k_B T} \tag{1.7}$$

(up to statistical-spin factors of order unity) [14]. At typical helium-core conditions $\rho \sim 10^5\,\mathrm{g\,cm^{-3}}$ and $k_B T \sim 15\,\mathrm{keV}$,

$$\frac{n(^8\mathrm{Be})}{n(^4\mathrm{He})} \sim 10^{-9}. \tag{1.8}$$

The exponential alone is $\mathrm{e}^{-92/15} \approx 2 \times 10^{-3}$; the remaining suppression is the density/thermal-wavelength prefactor. A non-resonant capture of a third α on that population would produce negligible cosmic carbon.

1.5.3 The Hoyle resonance and radiative branching

The capture

$$^8\mathrm{Be} + {^4\mathrm{He}} \to {^{12}\mathrm{C}^*} \to {^{12}\mathrm{C}} + \gamma \tag{1.9}$$

is rescued by the 0^+ **Hoyle state** of ^{12}C: 7654 keV above the ground state and only 287 keV above the $^8\mathrm{Be} + \alpha$ threshold. For $k_B T \sim 15\,\mathrm{keV}$ the Gamow energy is $E_\mathrm{G} \sim 200\,\mathrm{keV}$, so the resonance sits in the astrophysically sampled window [38, 14, 6]. Typical widths are $\Gamma_\alpha \approx 8.3\,\mathrm{eV}$ (return to $^8\mathrm{Be} + \alpha$) and $\Gamma_\gamma \sim 3 \times 10^{-3}\,\mathrm{eV}$ (electromagnetic decay toward bound ^{12}C), so only about one formation in 10^3–10^4 locks carbon permanently [14]. The net irreversible process is

$$3\,{^4\mathrm{He}} \to {^{12}\mathrm{C}}, \qquad Q = 7.27\,\mathrm{MeV}. \tag{1.10}$$

That resonance was predicted from the cosmic carbon abundance before it was measured in the laboratory [38, 6].

1.5.4 Helium-burning ashes: carbon and oxygen

Once ^{12}C is available, successive α captures compete with triple-α:

$$^{12}\mathrm{C} + {^4\mathrm{He}} \to {^{16}\mathrm{O}} + \gamma, \tag{1.11}$$

$$^{16}\mathrm{O} + {^4\mathrm{He}} \to {^{20}\mathrm{Ne}} + \gamma. \tag{1.12}$$

A helium-exhausted core is therefore typically a C/O mixture, with the C/O ratio sensitive to the still imperfectly known $^{12}\mathrm{C}(\alpha,\gamma)^{16}\mathrm{O}$ rate [14, 6, 1, 36]. That ratio later controls white-dwarf structure and Type Ia supernova yields.

1.6 Advanced burning in massive stars

When helium is exhausted, the C/O core contracts again. Only sufficiently massive stars reach carbon ignition and the subsequent stages (Fig. 1.3).

1.6.1 Carbon burning as a compound-nucleus branch

At $T \sim (5\text{–}9) \times 10^8\,\mathrm{K}$, two $^{12}\mathrm{C}$ nuclei form an excited $^{24}\mathrm{Mg}^*$ compound system that decays by γ, p or α emission [14]:

$$^{12}\mathrm{C} + {}^{12}\mathrm{C} \to {}^{20}\mathrm{Ne} + {}^{4}\mathrm{He} \quad (Q = 4.62\,\mathrm{MeV}), \tag{1.13}$$

$$\to {}^{23}\mathrm{Na} + p \quad (Q = 2.24\,\mathrm{MeV}), \tag{1.14}$$

$$\to {}^{24}\mathrm{Mg} + \gamma \quad (Q = 13.93\,\mathrm{MeV}). \tag{1.15}$$

The α and proton branches dominate over pure radiative capture. The liberated light particles are promptly absorbed by remaining carbon, feeding $^{13}\mathrm{N}$ and $^{16}\mathrm{O}$ and enriching the odd-A inventory.

1.6.2 Neon, oxygen and silicon burning

After carbon exhaustion the photon bath grows hard enough that photodisintegration begins to free α particles from neon and heavier ash. Neon burning is largely a rearrangement (γ, α) followed by α capture; oxygen burning again proceeds through compound channels analogous to carbon burning [14]. At still higher temperature ($T \sim 3 \times 10^9\,\mathrm{K}$) silicon burning becomes an α-particle quasi-equilibrium: photodisintegration maintains a population of α's that are captured in a ladder

$$^{28}\mathrm{Si} \xrightarrow{\alpha} {}^{32}\mathrm{S} \xrightarrow{\alpha} {}^{36}\mathrm{Ar} \cdots \xrightarrow{\alpha} {}^{56}\mathrm{Ni}, \tag{1.16}$$

after which $^{56}\mathrm{Ni}$ decays toward $^{56}\mathrm{Fe}$ [14, 37, 6]. Concurrent neutrino losses from pair and plasma processes shorten these advanced stages dramatically relative to hydrogen and helium burning [14].

Figure 1.3 is the geometric consequence: each exhausted fuel leaves an ash layer that ignites only after further gravitational heating, producing the classic onion of a pre-supernova massive star.

1.7 Why fusion stops at the iron peak

1.7.1 Binding-energy argument

The binding energy per nucleon B/A rises from light nuclei to a broad maximum near $A \sim 56$–62 and then falls slowly [6, 1]. For a fusion reaction $X + Y \to Z$,

$$Q = B(Z) - B(X) - B(Y) = A_Z \left(\frac{B}{A}\right)_Z - A_X \left(\frac{B}{A}\right)_X - A_Y \left(\frac{B}{A}\right)_Y. \tag{1.17}$$

If both reactants sit below the iron peak and the product remains near that peak, $Q > 0$. If both sit above it, $Q < 0$: hydrostatic fusion cannot power the star [6, 1, 14]. That is why Fig. 1.1

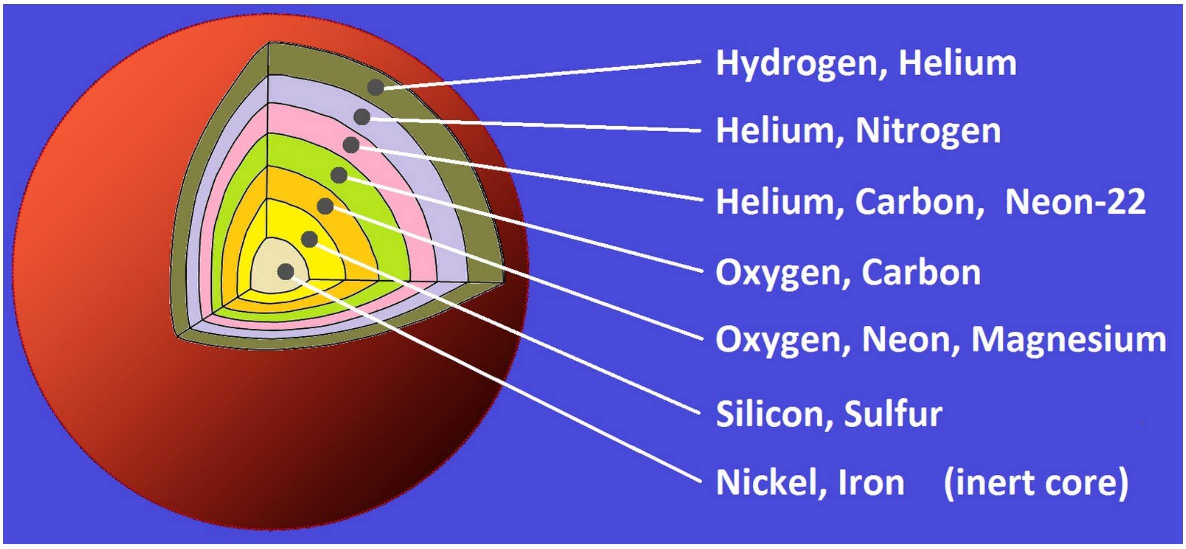

Figure 1.3: Original open-licence cutaway of a massive star near core collapse (onion-skin structure): nested burning shells of H/He, He/C, C/O, O/Ne/Mg, Si/S, surrounding an inert Ni/Fe core. Image: Wikimedia Commons ("Massive star cutaway pre-collapse"), CC0 [14, 6].

shows an iron-group abundance peak and why the onion of Fig. 1.3 ends in an inert Ni/Fe core.

1.7.2 Core collapse

Once silicon burning can no longer support the core against gravity, the iron core approaches the Chandrasekhar mass. Photodisintegration (γ, α and γ, n) and electron captures then cool and deleptonise the core, accelerating collapse. For a sufficiently massive progenitor the bounce and neutrino-driven explosion eject the outer onion and disseminate the synthesised nuclei into the interstellar medium, enriching the next generation of stars – including the Sun [14, 6, 1].

1.8 Side reactions: odd-A nuclei and free neutrons

α capture and even–even preference underproduce odd-A and odd-Z species unless side channels operate. Carbon-burning proton and α branches, followed by secondary captures, help populate those nuclides [14]. More important for the rest of the Periodic Table, some channels liberate free neutrons,

$$^{13}\mathrm{C} + {}^{4}\mathrm{He} \to {}^{16}\mathrm{O} + n, \qquad {}^{12}\mathrm{C} + {}^{12}\mathrm{C} \to {}^{23}\mathrm{Mg} + n \quad (Q = -2.6\,\mathrm{MeV}), \tag{1.18}$$

the second being endothermic but accessible at high temperature [14, 32]. Neutrons feel no Coulomb barrier: once a seed nucleus exists, successive (n, γ) reactions can increase A even when charged-particle fusion is forbidden by the iron peak.

1.9 Beyond iron: neutron capture (preview)

For $A \gtrsim 60$, charged-particle fusion is endothermic. Neutron capture followed by β^- decay changes both A and Z. Two limiting regimes are distinguished [37, 14, 6]:

- the **slow** (s) process, with capture timescales longer than β lifetimes, so the path hugs the valley of β stability;
- the **rapid** (r) process, with captures much faster than β decays, driving nuclei far to the neutron-rich side before they decay back after the neutron flux ends.

Abundance peaks near closed neutron shells ($N = 50, 82, 126$) are the signatures of both paths, shifted relative to each other because the r process β-decays into the valley from more neutron-rich progenitors. A minority of proton-rich rare isotopes require a separate p process (photodisintegration or neutrino processing of seed nuclei). The nuclear lesson of this chapter is that charged-particle stellar fusion builds the Periodic Table only through the iron group; neutrons carry nucleosynthesis the rest of the way [37, 6].

Key idea

- BBN: freeze-out $n/p \Rightarrow Y_{\mathrm{He}} \approx 2X_n/(1 + X_n) \approx 0.25$; $A \leq 7$ only.
- Abundances map nuclear structure: LiBeB gap, even–odd staggering, iron peak, s/r shell peaks.
- Triple-α: ^{8}Be Saha equilibrium + Hoyle resonance (287 keV above threshold) $\Rightarrow$ carbon.
- Massive-star onion ends at inert Fe/Ni; Q from B/A explains why.
- Free neutrons enable s/r capture beyond iron.

1.10 Further physics

Detailed balance origin of (1.7). Equating the $\alpha\alpha$ formation rate through a continuum T-matrix with the inverse decay $^8\mathrm{Be} \to 2\alpha$ and integrating over thermal Maxwellians cancels the unknown matrix element and leaves a Saha-like ratio controlled only by $Q = -92\,\mathrm{keV}$, reduced mass, and density [14]. The same logic underlies Saha ionisation in stellar atmospheres.

Partial widths of the Hoyle state. Typical values are $\Gamma_\alpha \sim 8\,\mathrm{eV}$ into the $\alpha + {}^8\mathrm{Be}$ channel and $\Gamma_\gamma \sim 3 \times 10^{-3}\,\mathrm{eV}$ into electromagnetic decay toward bound ^{12}C. The radiative branching $\Gamma_\gamma/\Gamma \sim 4 \times 10^{-4}$ makes carbon production rare per formation of $^{12}\mathrm{C}^*$, but still cosmically decisive once integrated over helium-burning lifetimes [14, 38].

Primary versus secondary nuclei. Species produced from primordial H/He alone (e.g. C,O in massive stars) are primary; those requiring seed metals from earlier generations (many s-process nuclei, CNO catalysts in Population I stars) are secondary. Abundance trends with metallicity distinguish the two [37, 14].

Connection to solar neutrinos. Hydrogen-burning rates that set solar neutrino fluxes (Lecture 27) are the first link of the same chain that later builds CNO catalysts and seeds for capture nucleosynthesis [36, 1].

1.11 Problems with solutions

Problem 28.1 — Helium mass fraction from X_n. Derive $Y_{\rm He} \approx 2X_n/(1+X_n)$. Evaluate it for $X_n = 1/8$ and for $X_n = 0.12$.

Solution 28.1. If every two neutrons (with two protons) form one ^{4}He, the helium mass is $4n_n/2 = 2n_n$ while the total baryon mass is $n_n + n_p$. With $X_n = n_n/(n_n + n_p)$ one obtains (1.3). For $X_n = 1/8$, $Y = 2/9 \approx 0.222$; for $X_n = 0.12$, $Y \approx 0.214$ before small network corrections raise the standard BBN result near 0.25 [14].

Problem 28.2 — ^{8}Be equilibrium. Starting from detailed balance for $^4\text{He}+{}^4\text{He} \rightleftharpoons {}^8\text{Be}$ with $Q = -92\,\text{keV}$, explain the exponential factor in (1.7) and estimate why $n(^8\text{Be})/n(^4\text{He}) \sim 10^{-9}$ at $k_BT = 15\,\text{keV}$.

Solution 28.2. The Boltzmann factor $\mathrm{e}^{-|Q|/k_BT}$ suppresses the unbound state; $\mathrm{e}^{-92/15} \approx \mathrm{e}^{-6.1} \approx 2\times10^{-3}$ already. The remaining $\sim 10^{-6}$ comes from the density and thermal wavelength prefactor in (1.7) at $\rho \sim 10^5\,\text{g}\,\text{cm}^{-3}$ [14].

Problem 28.3 — Why the Hoyle state matters. The Hoyle 0^+ lies 283 keV above the $^8\text{Be} + \alpha$ threshold. Why does that placement matter for helium burning at $k_BT \sim 15\,\text{keV}$?

Solution 28.3. The Gamow peak for $\alpha + {}^8\text{Be}$ sits near $E_{\rm G} \sim 200\,\text{keV}$ at that temperature, so a resonance 283 keV above threshold lies in the astrophysically sampled window and enhances the rate by many orders of magnitude relative to a non-resonant extrapolation [38, 14, 6].

Problem 28.4 — Fusion Q from B/A. Using (1.17), argue schematically why $^{28}\text{Si} + {}^{28}\text{Si} \to {}^{56}\text{Ni}$ can release energy while $^{56}\text{Fe} + {}^{56}\text{Fe} \to {}^{112}\text{Cd}$ cannot power a star.

Solution 28.4. Near $A \sim 28$, B/A is still rising toward the iron peak, so the fused product has larger B/A and $Q > 0$. Near $A \sim 56$, B/A is maximal or already declining, so fusing two iron-group nuclei decreases the average binding and $Q < 0$ [6, 1].

Problem 28.5 — Reading the onion figure. Using Fig. 1.3, list the shells from outside in and state which stage of burning produced each ash layer.

Solution 28.5. Outer H/He (H burning ash and envelope); He/C/Ne (helium burning); C/O (carbon burning products); O/Ne/Mg (neon burning); Si/S (oxygen/silicon burning); central Ni/Fe (inert core). Each inner shell requires a higher ignition temperature than the one outside it [14].

Problem 28.6 — Why no carbon in BBN? Explain why Big Bang nucleosynthesis stops short of carbon even though helium is abundant.

Solution 28.6. No stable $A = 5, 8$ bridge exists; the ^{8}Be equilibrium needed for triple-α requires stellar densities sustained far longer than the minutes available in BBN [14, 6].

Bibliography

[1] R. A. Dunlap, *An Introduction to the Physics of Nuclei and Particles* (2nd ed.), IOP Publishing, Bristol (2023), DOI: 10.1088/978-0-7503-6094-4, Ch. 3 (Nuclear composition and size).

[2] W. Demtröder, *Nuclear and Particle Physics*, Undergraduate Lecture Notes in Physics, Springer, Cham (2023).

[3] S. Petrera, *Problems and Solutions in Nuclear and Particle Physics*, UNITEXT for Physics, Springer, Cham (2019).

[4] F. Terranova, *A Modern Primer in Particle and Nuclear Physics*, Oxford University Press (2021).

[5] S. D'Auria, *Introduction to Nuclear and Particle Physics*, Undergraduate Lecture Notes in Physics, Springer, Cham (2018).

[6] K. S. Krane, *Introductory Nuclear Physics*, Wiley, New York (1988).

[7] R. Hofstadter, "Electron scattering and nuclear structure," Rev. Mod. Phys. **28**, 214 (1956).

[8] H. F. Ehrenberg, R. Hofstadter, U. Meyer-Berkhout, D. G. Ravenhall, and S. E. Sobottka, "High-Energy Electron Scattering and the Charge Distribution of Carbon-12 and Oxygen-16," Phys. Rev. **113**, 666 (1959).

[9] H. Yukawa, "On the interaction of elementary particles. I," Proc. Phys.-Math. Soc. Japan **17**, 48 (1935).

[10] R. D. Woods and D. S. Saxon, "Diffuse surface optical model for nucleon-nuclei scattering," Phys. Rev. **95**, 577 (1954).

[11] H. G. J. Moseley, "The high-frequency spectra of the elements," Phil. Mag. **26**, 1024 (1913); **27**, 703 (1914).

[12] C. F. von Weizsäcker, "Zur Theorie der Kernmassen," Z. Phys. **96**, 431 (1935).

[13] P. Cappellaro, *Introduction to Applied Nuclear Physics* (MIT OpenCourseWare / LibreTexts), CC BY-NC-SA 4.0.

[14] J.-L. Basdevant, J. Rich, and M. Spiro, *Fundamentals in Nuclear Physics: From Nuclear Structure to Cosmology*, Springer, New York (2005).

[15] D. Tong, *Particle Physics*, Lecture notes (University of Cambridge / CERN school notes).

[16] M. G. Mayer, "On closed shells in nuclei. II," Phys. Rev. **75**, 1969 (1949).

[17] O. Haxel, J. H. D. Jensen, and H. E. Suess, "On the "magic numbers" in nuclear structure," Phys. Rev. **75**, 1766 (1949).

[18] T. Schmidt, "Über die magnetischen Momente der Atomkerne," Z. Phys. **106**, 358 (1937).

[19] L. W. Nordheim, "On spins, moments, and shells in nuclei," Phys. Rev. **78**, 294 (1950).

[20] Evaluated Nuclear Structure Data File (ENSDF), National Nuclear Data Center, Brookhaven National Laboratory, `https://www.nndc.bnl.gov/ensdf/`.

[21] NuDat 3, National Nuclear Data Center, Brookhaven National Laboratory, `https://www.nndc.bnl.gov/nudat3/`.

[22] N. J. Stone, "Table of nuclear magnetic dipole and electric quadrupole moments," At. Data Nucl. Data Tables **90**, 75 (2005); updated compilations at NNDC.

[23] W. N. Cottingham and D. A. Greenwood, *An Introduction to Nuclear Physics* (2nd ed.), Cambridge University Press, Cambridge (2001).

[24] H. Geiger and J. M. Nuttall, "The ranges of the α particles from the radioactive substances," Phil. Mag. **22**, 613 (1911).

[25] G. Gamow, "Zur Quantentheorie des Atomkernes," Z. Phys. **51**, 204 (1928).

[26] R. W. Gurney and E. U. Condon, "Wave mechanics and radioactive disintegration," Nature **122**, 439 (1928); Phys. Rev. **33**, 127 (1929).

[27] M. Wang, W. J. Huang, F. G. Kondev, G. Audi, and S. Naimi, "The AME 2020 atomic mass evaluation (II). Tables, graphs and references," Chin. Phys. C **45**, 030003 (2021).

[28] Laboratoire National Henri Becquerel (LNHB), Recommended decay data, `http://www.lnhb.fr/nuclear-data/nuclear-data-table/`.

[29] L. M. Langer, R. D. Moffat, and H. C. Price, Jr., "Low energy beta-ray spectra: P^{32} and Cu^{64}," Phys. Rev. **76**, 1725 (1949).

[30] L. M. Langer and H. C. Price, Jr., "Shapes of the beta-spectra of the forbidden transitions of Sb^{124}, Rb^{86}, Sr^{89}, Y^{91}, and Cs^{137}," Phys. Rev. **75**, 1769 (1949).

[31] D. C. Camp and L. M. Langer, "The shape of the ^{66}Ga positron spectrum and the contribution from $0^+ \to 0^+$ transitions," Phys. Rev. **129**, 1782 (1963).

[32] H. C. Verma, *Nuclear Physics: Fundamentals and Applications*, NPTEL/IIT Kanpur lecture series, `https://hcverma.in/ncl_phy_lectures`.

[33] International Atomic Energy Agency, *LiveChart of Nuclides*, evaluated structure, decay, reaction, and fission-yield data, `https://www-nds.iaea.org/relnsd/vcharthtml/VChartHTML.html`.

[34] T. Kibédi, T. W. Burrows, M. B. Trzhaskovskaya, P. M. Davidson, and C. W. Nestor, Jr., "Evaluation of theoretical conversion coefficients using BrIcc," Nucl. Instrum. Methods Phys. Res. A **589**, 202 (2008), DOI: 10.1016/j.nima.2008.02.051.

[35] D. A. Brown *et al.*, "ENDF/B-VIII.0: The 8th major release of the nuclear reaction data library with CIELO-project cross sections, new standards and thermal scattering data," Nucl. Data Sheets **148**, 1 (2018), DOI: 10.1016/j.nds.2018.02.001.

[36] B. Acharya *et al.*, "Solar fusion III: New data and theory for hydrogen-burning stars," Rev. Mod. Phys. **97**, 035002 (2025), DOI: 10.1103/8lm7-gs18.

[37] E. M. Burbidge, G. R. Burbidge, W. A. Fowler, and F. Hoyle, "Synthesis of the elements in stars," Rev. Mod. Phys. **29**, 547 (1957), DOI: 10.1103/RevModPhys.29.547.

[38] F. Hoyle, "On Nuclear Reactions Occurring in Very Hot Stars. I. The Synthesis of Elements from Carbon to Nickel," Astrophys. J. Suppl. **1**, 121 (1954), DOI: 10.1086/190005.

[39] S. N. Ghoshal, "An experimental verification of the theory of compound nucleus," Phys. Rev. **80**, 939 (1950), DOI: 10.1103/PhysRev.80.939.

[40] D. Adhikari *et al.* (PREX Collaboration), "Accurate determination of the neutron skin thickness of ^{208}Pb through parity-violation in electron scattering," Phys. Rev. Lett. **126**, 172502 (2021), DOI: 10.1103/PhysRevLett.126.172502.

[41] B. T. Reed, F. J. Fattoyev, C. J. Horowitz, and J. Piekarewicz, "Implications of PREX-II on the equation of state of neutron-rich matter," Phys. Rev. Lett. **126**, 172503 (2021), DOI: 10.1103/PhysRevLett.126.172503.

[42] B. Hu *et al.*, "Ab initio predictions link the neutron skin of ^{208}Pb to nuclear forces," Nature Phys. **18**, 1196 (2022), DOI: 10.1038/s41567-022-01715-8.

[43] E. Epelbaum, H.-W. Hammer, and U.-G. Meißner, "Modern theory of nuclear forces," Rev. Mod. Phys. **81**, 1773 (2009), DOI: 10.1103/RevModPhys.81.1773.

[44] H.-W. Hammer, S. König, and U. van Kolck, "Nuclear effective field theory: Status and perspectives," Rev. Mod. Phys. **92**, 025004 (2020), DOI: 10.1103/RevModPhys.92.025004.

[45] T. Otsuka, A. Gade, O. Sorlin, T. Suzuki, and Y. Utsuno, "Evolution of shell structure in exotic nuclei," Rev. Mod. Phys. **92**, 015002 (2020), DOI: 10.1103/RevModPhys.92.015002.

[46] H. Hergert, S. K. Bogner, T. D. Morris, A. Schwenk, and K. Tsukiyama, "The in-medium similarity renormalization group: A novel ab initio method for nuclei," Phys. Rep. **621**, 165 (2016), DOI: 10.1016/j.physrep.2015.12.007.

[47] J. M. Lattimer and M. Prakash, "The equation of state of hot, dense matter and neutron stars," Phys. Rep. **621**, 127 (2016), DOI: 10.1016/j.physrep.2015.12.005.

[48] J. M. Lattimer, "Neutron stars and the nuclear matter equation of state," Annu. Rev. Nucl. Part. Sci. **71**, 433 (2021), DOI: 10.1146/annurev-nucl-102419-124827.

[49] B. P. Abbott *et al.* (LIGO Scientific Collaboration and Virgo Collaboration), "GW170817: Observation of gravitational waves from a binary neutron star inspiral," Phys. Rev. Lett. **119**, 161101 (2017), DOI: 10.1103/PhysRevLett.119.161101.

[50] M. J. Dolinski, A. W. P. Poon, and W. Rodejohann, "Neutrinoless double-beta decay: Status and prospects," Annu. Rev. Nucl. Part. Sci. **69**, 219 (2019), DOI: 10.1146/annurev-nucl-101918-023407.

[51] M. Agostini, G. Benato, J. A. Detwiler, J. Menéndez, and F. Vissani, "Toward the discovery of matter creation with neutrinoless $\beta\beta$ decay," Rev. Mod. Phys. **95**, 025002 (2023), DOI: 10.1103/RevModPhys.95.025002.

[52] P. Gysbers *et al.*, "Discrepancy between experimental and theoretical β-decay rates resolved from first principles," Nature Phys. **15**, 428 (2019), DOI: 10.1038/s41567-019-0450-7.

[53] H. L. Crawford, K. Fossez, S. König, and A. Spyrou, "A vision for the science of rare isotopes," Annu. Rev. Nucl. Part. Sci. **74**, 141 (2024), DOI: 10.1146/annurev-nucl-121423-091501.

[54] Nuclear Science Advisory Committee, *A New Era of Discovery: The 2023 Long Range Plan for Nuclear Science*, U.S. Department of Energy and National Science Foundation (2023), `https://nuclearsciencefuture.org/`.

[55] S. A. Giuliani, Z. Matheson, W. Nazarewicz, E. Olsen, P.-G. Reinhard, J. Sadhukhan, B. Schuetrumpf, N. Schunck, and P. Schwerdtfeger, "Colloquium: Superheavy elements: Oganesson and beyond," Rev. Mod. Phys. **91**, 011001 (2019), DOI: 10.1103/RevModPhys.91.011001.

[56] N. Schunck and D. Regnier, "Theory of nuclear fission," Prog. Part. Nucl. Phys. **125**, 103963 (2022), DOI: 10.1016/j.ppnp.2022.103963.

[57] I. Counts, J. Hur, D. P. L. Aude Craik, H. Jeon, C. Leung, J. C. Berengut, A. Geddes, A. Kawasaki, W. Jhe, and V. Vuletić, "Evidence for nonlinear isotope shift in Yb^+ search for new boson," Phys. Rev. Lett. **125**, 123002 (2020), DOI: 10.1103/PhysRevLett.125.123002.

[58] I. Angeli and K. P. Marinova, "Table of experimental nuclear ground state charge radii: An update," At. Data Nucl. Data Tables **99**, 69 (2013), DOI: 10.1016/j.adt.2011.12.006.

[59] S. Kraemer *et al.*, "Observation of the radiative decay of the ^{229}Th nuclear clock isomer," Nature **617**, 706 (2023), DOI: 10.1038/s41586-023-05894-z.